

Article

Thermal Properties of Porous Mullite Ceramics Modified with Microsized ZrO₂ and WO₃

Ludmila Mahnicka-Goremikina ^{1,*}, Ruta Svinka ¹, Visvaldis Svinka ¹, Liga Grase ¹, Inna Juhneva ¹, Maris Rundans ¹, Vadims Goremikins ², Sanat Tolendiuly ³ and Sergey Fomenko ⁴

¹ Institute of Materials and Surface Engineering, Faculty of Materials Science and Applied Chemistry, Riga Technical University, Paula Valdena St. 3/7, LV-1048 Riga, Latvia

² Institute of Structural Engineering and Reconstruction, Riga Technical University, Kipsalas St. 6A, LV-1048 Riga, Latvia

³ Space Engineering Department, AUPET Named G. Daukeev, Baitursynov St., 126/1, Almaty 050013, Kazakhstan

⁴ Institute of Combustion Problems, Bogenbay Batyr St. 172, Almaty 050012, Kazakhstan

* Correspondence: mahnicka@inbox.lv



Citation: Mahnicka-Goremikina, L.; Svinka, R.; Svinka, V.; Grase, L.; Juhneva, I.; Rundans, M.; Goremikins, V.; Tolendiuly, S.; Fomenko, S. Thermal Properties of Porous Mullite Ceramics Modified with Microsized ZrO₂ and WO₃. *Materials* **2022**, *15*, 7935. <https://doi.org/10.3390/ma15227935>

Academic Editors: Andres Sotelo, Zhifeng Wang, Weiqing Zhang and Yichao Wang

Received: 20 October 2022

Accepted: 7 November 2022

Published: 10 November 2022

Publisher's Note: MDPI stays neutral with regard to jurisdictional claims in published maps and institutional affiliations.



Copyright: © 2022 by the authors. Licensee MDPI, Basel, Switzerland. This article is an open access article distributed under the terms and conditions of the Creative Commons Attribution (CC BY) license (<https://creativecommons.org/licenses/by/4.0/>).

Abstract: Mullite ceramics are well known as materials with a high temperature stability, strength and creep resistance. In this research, the effect of a modification with magnesia-stabilized zirconia and yttria-stabilized zirconia, separately, as well as in a mixture with WO₃, in 1:1 and 1:2 ratios on the thermal properties of porous mullite ceramics was investigated. The porous mullite-containing ceramics were prepared by a slip casting of the concentrated slurry of raw materials with the addition of a suspension of Al paste for the pore formation due to the H₂ evolution as a result of the reaction of Al with water. The formed samples were sintered at 1600 °C and the holding time was 1 h. The materials were characterized using X-ray diffractometry, scanning electron microscopy, mercury porosimetry, the laser flash contactless method, thermal shock resistance testing and the non-destructive impulse excitation method for determining the elasticity modulus. The modification of the porous mullite ceramic with a mixture of ZrO₂ and WO₃ oxides had a positive effect by decreasing the thermal conductivity, due to the increased porosity, in comparison to the undoped samples and samples with only ZrO₂. The doubling of the WO₃ amount in the modifying oxide mixtures improved the ceramic thermal shock resistance. The porous mullite ceramics which were modified with magnesia-stabilized zirconia (2.8 mol% MgO) and WO₃ had a lower thermal conductivity and improved thermal shock resistance than the samples with yttria-stabilized zirconia (8 mol% Y₂O₃) and WO₃.

Keywords: mullite; porous ceramic; zirconia; tungsten oxide; thermal conductivity; thermal shock

1. Introduction

Special materials are needed to save thermal energy in the working space of thermal high-temperature units and prevent it from flowing into the environment. Such materials are called high-temperature thermal insulation materials. Thermal energy losses during high-temperature processes often exceed its theoretical need by several times. Climate-neutral manufacturing aims to boost the efficient use of fossil and energy resources by reducing air and water pollution, reducing heat losses and slowing down climate change. The investigation and use of porous high-temperature ceramics for thermal insulation help to achieve the goals of climate-neutral manufacturing and decrease the environmental degradation [1–4].

Ceramic materials such as corundum, cordierite, zirconia, mullite and multiphase composite ceramics are used for high-temperature engineering applications. In order to apply these ceramic materials, it is important to take into account their thermal properties such as their thermal conductivity, specific heat capacity, thermal expansion coefficient,

resistance to sudden changes in temperature, thermal shock cracking and thermal shock induced fracture, as well as their mechanical properties [5–13].

Several layers of ceramic refractory material with different thermal resistances and thermal conductivities or ceramic composite materials with gradient properties are applied often in attempt to meet the aim of limiting the heat loss of certain equipment. For example, the cement kiln body can be divided into three layers, the working layer, the thermal-preservation layer and the thermal-insulation layer [6,7,14,15]. Layers can be made from different ceramic materials. Each layer has different thermal properties and its own role. The main properties of the working layer are its high thermal shock resistance, low thermal conductivity, high strength and long lifetime. The thermal-preservation layer must also have a high strength and lower thermal conductivity. The thermal-insulation layer has an ultra-low thermal conductivity to prevent heat loss and ensure the thermal protection of the other layers. The same situation is encountered in the thermal insulation of a spacecraft, where the thermal insulation consists of several layers [8–12,14]. Chen al. investigated the specific facing from composite material–multilayer mullite-based brick and porous plates, in which the thermal properties change along a gradient [6]. It is difficult to choose layers of materials or form a composite material such that the materials' components are physically and chemically compatible with one another. In addition, layering increases the load on the construction. It is important that there is no peeling or destruction during the operation under elevated temperature conditions [6–9]. In the case where thermal-insulating ceramics are used at high temperatures or extreme conditions, such as rapid increase and decrease in temperature, the introduced thermal shock may produce microcracks, whose growth and development can cause the structural failure of the component [10,11].

In terms of the economy and technology, it is beneficial when the insulation part of the thermal technical equipment and spaceships consists of one type of material with a low bulk density that combines a lot of functions and properties. There are difficulties in searching for ceramic candidates for thermal insulators. The first is the selection of a ceramic material oxide or composition of oxides that will have a low thermal conductivity. The second difficulty is achieving a low bulk density due to the certain porosity. The presence of pores with an effective pore size leads to a significant reduction in the thermal conductivity compared to a dense material. The third difficulty is obtaining ceramic materials that will simultaneously have low parameters, such as linear thermal expansion coefficients and thermal conductivity coefficients [13,16]. The use of multi-phase polycrystalline ceramics can solve this problem. It is also important to take into account the specific heat capacity of heat insulation ceramics. The specific heat capacity is defined as the quantity of heat absorbed per unit mass of the material when its temperature increases by 1 K [17]. More heat energy is required to increase the temperature of materials with a high specific heat capacity than ones with a low specific heat capacity. Depending on the purpose of the ceramics, the high or low specific heat capacity and thermal diffusivity of the ceramics must be taken into account [17–19].

Porous mullite-containing refractory ceramics are good candidates for a high-temperature thermal insulation and for reducing heat losses. Porous mullite-containing ceramics have a significant share in the field of technical ceramics for industrial and space fields [1,2,5]. The catalyst supports, filters for hot gases and molten metals, parts of burners, heat insulators of industrial furnaces, technical equipment and spaceships are produced from this type of ceramic. The choice of a refractory material for an application will be determined by the type of required functionality of the furnace, heating unit or refractory insulator component and the prevailing conditions, e.g., the gaseous atmosphere, the presence of slags and the type of metal charge [1,15,16,20–22].

In order to improve the mullite-containing ceramics, researchers investigated the influence of modifying such ceramics with different oxides on the thermal properties. Xu et al. sintered a cordierite–mullite–corundum composite with added Sm_2O_3 and achieved an increase in the thermal shock resistance and a decrease in the thermal conductivity (6.81 W/mK) and thermal expansion ($5.96 \times 10^{-6} \text{ }^\circ\text{C}^{-1}$) [23]. Li et al. synthesized columnar

self-reinforced mullite porous ceramics by adding V_2O_5 at 1350–1550 °C and achieved a porosity of about 63% and a thermal conductivity of about 1.04 W/mK [24]. The use of Ho_2O_3 [25], Gd_2O_3 [26] and HfO_2 [27] improved the thermal shock resistance and thermal durability of mullite-containing ceramics. There is still ongoing research related to the investigation of and improvement in the thermo-mechanical properties of mullite and alumina–mullite ceramic composites with zirconia or zirconia–zircon components [28–33]. The thermal conductivity, thermal diffusivity and specific heat capacity of ceramic samples could be obtained using different international test standards, provided in Table 1.

Table 1. Thermal analysis tests.

Thermal Analysis Tests	References
Standard test method for thermal conductivity and thermal diffusivity by modulated temperature differential scanning calorimetry.	[34,35]
Standard test method for determining specific heat capacity by differential scanning calorimetry.	[36,37]
Hot-plate system. Guarded hot-plate systems are used to measure steady-state heat flow through materials with low thermal conductivity (insulators).	[38–42]
Heat flow system. Guarded Comparative–Longitudinal Heat Flow Technique.	[42,43]
The laser flash method and laser pulse: Laser Flash Thermal Conductivity.	[42,44,45]

The application of WO_3 as an additive or raw component for the formation of an additional crystalline phase is relevant in different fields such as gas sensing, chromogenic, photocatalytic and emerging applications (biomedical, antibiotic and artificial intelligence) [46]. The use of WO_3 for a ceramic modification has not been extensively investigated. The main aim of the research work was the formation of the thermal-insulating mullite ceramic material with a high porosity, a high thermal shock resistance, at the same time as low linear thermal expansion coefficients, low thermal conductivity coefficients and a low specific heat capacity. The main tasks of the investigation were the modification of porous mullite ceramic with ZrO_2 and WO_3 oxides and the analysis of the thermal properties depending on the chemical compositions, structural features, porosity and pore morphology. Such ceramic materials will help reduce the heat loss and withstand the rapid temperature fluctuations [9,12–16].

2. Materials and Methods

2.1. Materials

Two types of aluminas, $\alpha-Al_2O_3$ ($d_{50} = 2 \mu m$) and $\gamma-Al_2O_3$ ($d_{50} = 80 \mu m$), were purchased from Nabalox, Nabaltec AG, Schwandorf, Germany. Kaolin ($d_{50} = 1.5 \mu m$; SiO_2 —56.5 wt.%, Al_2O_3 —31.0 wt.%) was purchased from MEKA, Amberger Kaolinwerke, Hirschau, Germany. The magnesia-stabilized zirconia (2.8 mol% MgO) with $d_{50} = 0.8 \mu m$ was obtained from Goodfellow, Huntingdon, UK. The yttria-stabilized zirconia (8 mol% Y_2O_3) with $d_{50} = 0.5 \mu m$, SiO_2 amorphous with $d_{50} = 3–5 \mu m$ and WO_3 with $d_{50} = 5 \mu m$ were acquired from GetNanoMaterials, Saint-Cannat, France. Aluminum paste (solid content of $70 \pm 2\%$) with $d_{50} = 12 \mu m$ was purchased from Aquapor-9008, Schlenk Metallic Pigments GmbH, Roth, Germany.

2.2. Material Proportions

The base of the mullite ceramic was prepared from two types of aluminas ($\alpha-Al_2O_3$ and $\gamma-Al_2O_3$), amorphous SiO_2 and kaolin. The ratio of Al_2O_3 to SiO_2 was 2.57:1 due to the mullite stoichiometric composition. The quantity of $\gamma-Al_2O_3$ was three times more than the quantity of $\alpha-Al_2O_3$. Kaolin was used at 30 wt.%. Oxides such as yttria-stabilized zirconia

(8 mol% Y_2O_3), magnesia-stabilized zirconia (2.8 mol% MgO) and WO_3 were used for the ceramic modifications. Both oxides were also used together in a mixture for modifying the mullite ceramics. The ratios of the different stabilized zirconia and tungsten oxide were 1:1 and 1:2.

2.3. Sample Preparation Methods

A slip casting of the concentrated slurry of raw materials was used for the sample preparation. The water content of the concentrated slurry was 38–40 wt.%. First, the dry raw materials were mixed in a dry state. Then, its suspension was created with distilled water and mixed for 10 min with a mechanical mixer to obtain a uniform particle distribution in the slurry. The suspension of aluminum paste was added into the raw material suspension and mixed for about 7–10 min. Then, the raw material slurry was slip casted into the mold. The porosity of the mullite ceramics was obtained due to the hydrogen gas evolution as a result of the reaction between the aluminum paste and water. The formed initial pores became visually noticeable 15–20 min after the slip casting. The pore formation took 1 to 3 h. After that, the samples were dried for 24 h at 20–25 °C and then for 24 h at 100 °C. The dried samples were sintered at 1600 °C with a 250 °C/h (4.2 °C/min) heating rate, and the holding time at the maximum temperature was 1 h. The cooling process of the fired samples was as slow as the heating process.

2.4. XRD Analysis

The phase compositions of the sintered materials were characterized by X-ray diffraction analysis (XRD; Rigaku Ultima + (Japan)) with CuK_{α} radiation, a voltage on the Cu anode of 30 kV, a current intensity of 20 mA, a range of the measurement angle of 5–60 $2\theta^{\circ}$ and a speed of the goniometer of 2°/min).

2.5. SEM Analysis

The morphology of the prepared samples was observed by using scanning electron microscopes: a TableTop SEM Hitachi TM3000 (Japan) at an electron beam energy of 5 keV and 15 keV, and a high-resolution SEM FEI Nova NanoSEM 650 (the Netherlands) at an electron beam energy of 10 keV. Metal coating sputtering was not used because the structures were observed in the low vacuum mode.

2.6. Apparent Porosity

The apparent porosity was mathematically calculated and based on the Archimedes' principle (European standard EN 623-2) after soaking the samples in distilled water. The apparent porosity P is the ratio of the total volume of the open pores in a porous body to its bulk volume. The apparent porosity P was calculated as a percentage using the following Equation (1):

$$P = ((m_3 - m_1)/(m_3 - m_2)) \times 100, \quad (1)$$

where m_1 is the mass of the dry test piece in grams, m_2 is the apparent mass of the immersed test piece in grams and m_3 is the mass of the soaked test piece in grams.

2.7. Hg Porosimetry

The pore size distribution of the porous mullite ceramic was analyzed by a mercury porosimeter (Quantachrome, Pore Master 33, USA). Mercury intrusion porosimetry makes it possible to obtain data on the pores in a material in a limited range from 0.006 μm to 1000 μm .

2.8. Thermal Analysis

The specific heat capacity and thermal conductivity measurements and the calculation of the thermal diffusivity of the samples were carried out using the laser flash contactless method using the universal equipment table-top instrument Netzsch LFA 457 MicroFlash,

Germany. The measurements were carried out in the temperature range from 25 °C to 1100 °C. The sample dimensions were 10 mm × 10 mm and the thickness was 3 mm.

Thermal diffusivity (α with the unit mm²/s) is a material-specific property for characterizing an unsteady heat conduction. This value describes how fast heat diffuses through the material. The thermal diffusivity was calculated from the following Equation (2):

$$\alpha = \kappa / (\rho C_p), \quad (2)$$

where κ is the thermal conductivity (W/(m·K)), ρ is the density (kg/m³) and C_p is the specific heat capacity (J/kg/K) [18,19].

2.9. Thermal Shock Resistance Testing

The thermal shock resistance of the ceramics was determined during 10 cycles of thermal shock corresponding to the scheme 20 °C → 1000 °C → 20 °C with an exposure for 1 h at 1000 °C.

2.10. Elasticity Modulus Determination

The change in the elasticity modulus was measured before and after the 1st, 2nd, 5th and 10th thermal shock test by a non-destructive impulse excitation method (equipment Buzz-O-Sonic 5.0; BuzzMac International, LLC, USA). The non-destructive method provides an opportunity to examine the same sample after each thermal shock cycle, which allowed for more precise results.

3. Results and Discussion

3.1. Mineralogical Phase Composition

The XRD patterns of the prepared materials are shown in Figures 1 and 2. Comparing the experimental diffraction pattern with those from the International Centre of Diffraction Data (ICDD), the crystalline phases of the undoped samples correspond to mullite and corundum (Figure 1a).

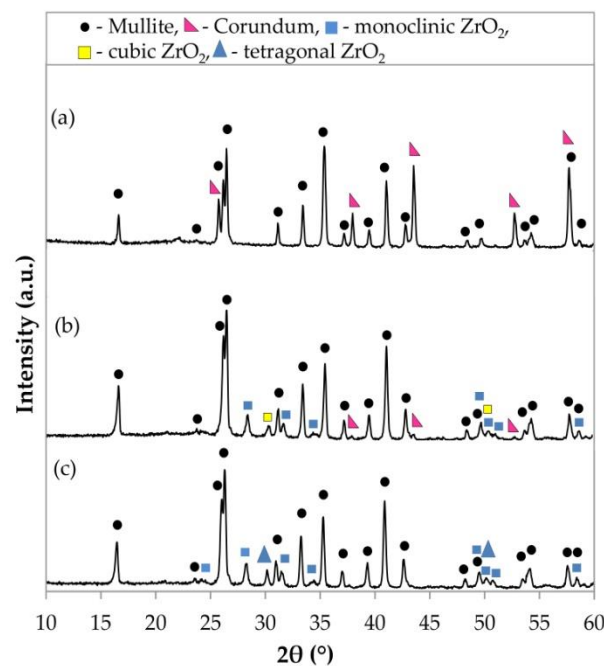


Figure 1. X-ray diffraction data of the sintered porous ceramic materials: (a) undoped samples, (b) samples with YSZ and (c) samples with MSZ.

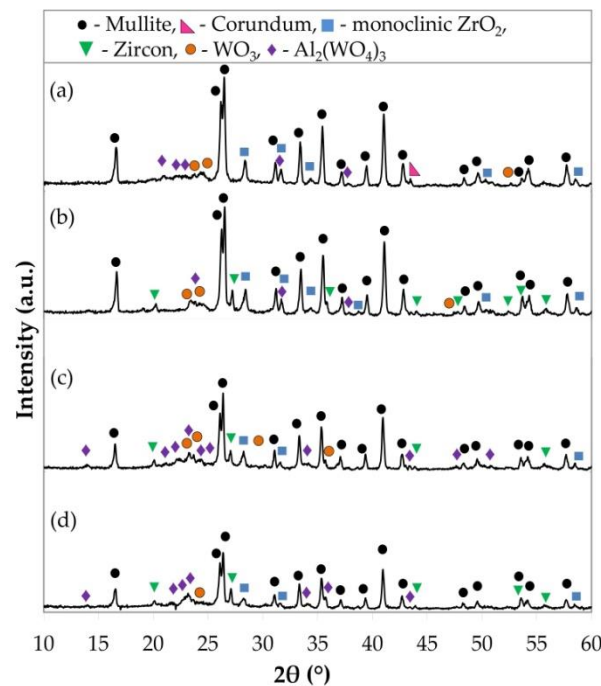


Figure 2. X-ray diffraction data of the sintered porous ceramic materials: (a) with YSZ:WO₃ (1:1), (b) with MSZ:WO₃ (1:1), (c) with YSZ:WO₃ (1:2) and (d) with MSZ:WO₃ (1:2).

The samples with yttria-stabilized zirconia and magnesia-stabilized zirconia contained mullite and monoclinic and tetragonal ZrO₂ (Figure 1b,c). The corundum phase remained in the samples with YSZ. The XRD patterns (Figure 2a,b) of the samples with a mixture of YSZ or MSZ and WO₃ in a 1:1 ratio show the presence of mullite, monoclinic ZrO₂, WO₃ and aluminum tungstate in both the materials of such compositions. Zircon was formed additionally in samples with MSZ and WO₃ (1:1).

The samples with a mixture of YSZ or MSZ and WO₃ in a 1:2 ratio have the main phase, the mullite phase (Figure 2c,d), as well as such phases as monoclinic ZrO₂, zircon and aluminum tungstate. The presence of WO₃ in the compositions with MSZ and WO₃ (1:2) was less pronounced than in the samples with YSZ and WO₃ (1:2). A detailed description of the crystalline phase formation was considered in a previous investigation, which was described in the article [47].

3.2. Macrostructure

The images of the porous mullite ceramic surface were obtained using a Table Top SEM and $\times 20$ magnification (Figure 3). The pores have a spherical shape and approximately the same cross section as in the samples without the addition of modifying oxides (Figure 3a).

The pores of the modified samples only with YSZ or MSZ as well as with these oxides and WO₃ mixtures do not have the strong spherical form with a uniform diameter. All samples with modifying oxide additives are characterized by an elongated pore shape in the ceramic structure. It is important to note that these elongated pores are characterized by an expressed orientation in the ceramic structure. Such elongation and orientation occurred in the direction parallel to the base of the molds, respectively, parallel to the horizontal plane of the samples or along the sample length. When analyzing the photo of the surface of the modified samples along the pores and across the pores, it can be seen that to a greater extent, the pores are isolated from each other. The pores have slit shapes with a partial networking because they have a joint intersection and branching, as well as a stomach and dead ends (Figure 3b–g). The length of the pores is 2–3 times greater than their width and height. The walls of the pores are not smooth but uneven due to the fact that large pores are formed from the merging of several smaller pores.

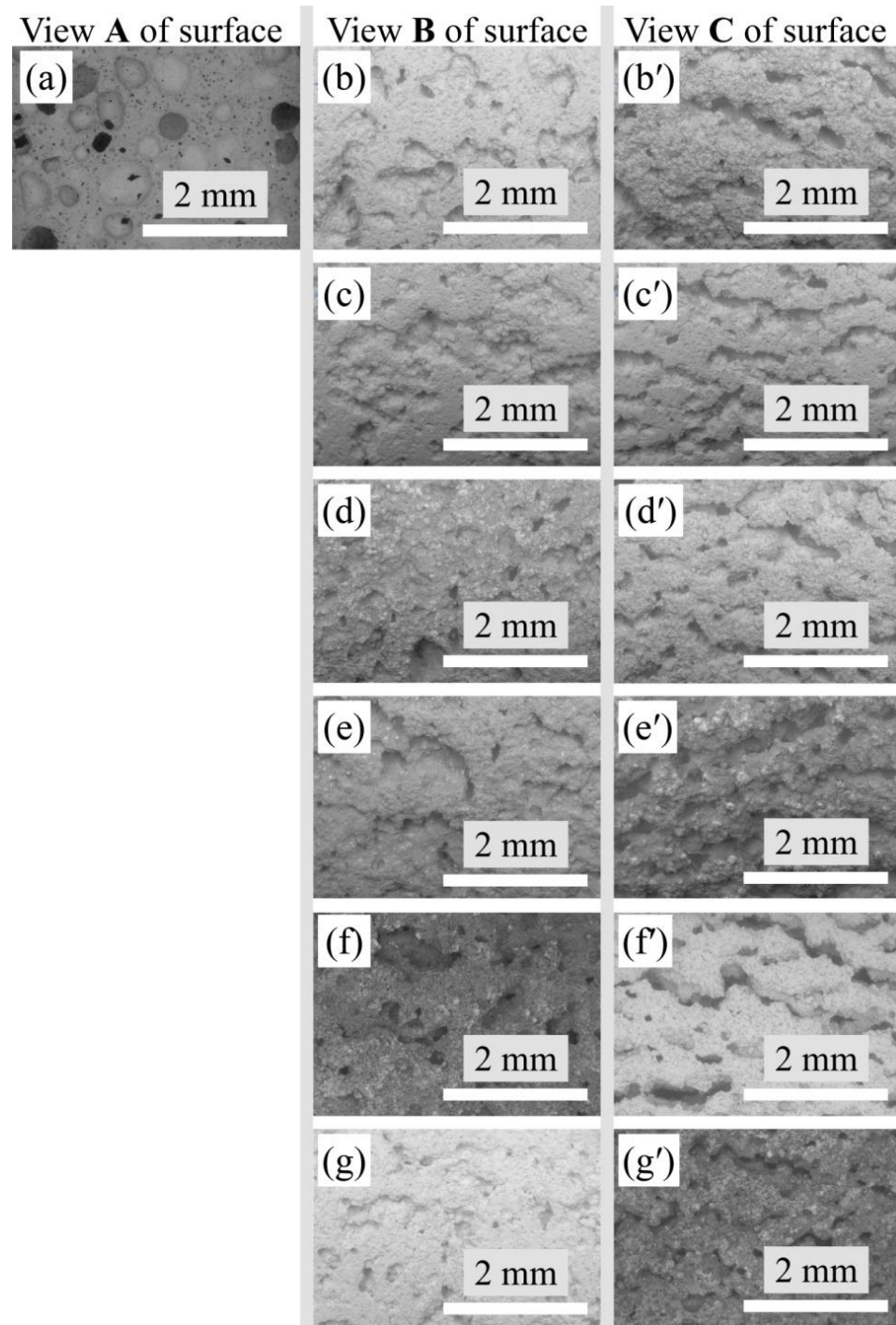


Figure 3. TableTop SEM micrographs illustrating the macrostructure of the investigated samples, magnification $\times 20$: (a) view A of the undoped sample surface; (b–g) view B of the modified sample surface perpendicular to the base of the molds; (b'–g') view C of the modified sample surface parallel to the base of the molds; (b,b') samples with YSZ; (c,c') with MSZ; (d,d') with YSZ:WO₃ (1:1); (e,e') with MSZ:WO₃ (1:1); (f,f') with YSZ:WO₃ (1:2); and (g,g') with MSZ:WO₃ (1:2).

3.3. Microstructure

The microstructure of the porous mullite ceramic without a modifying additive and only with yttria-stabilized zirconia or magnesia-stabilized zirconia formed from densely packed and closely bordered crystals is shown in Figure 4.

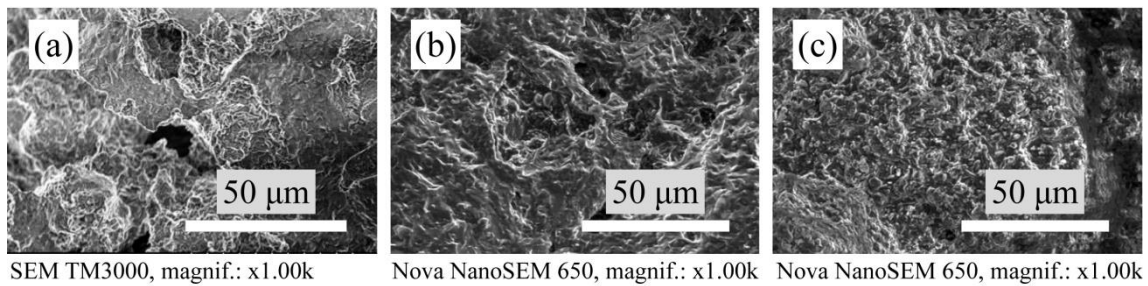


Figure 4. SEM micrographs of the microstructure of sintered samples: (a) undoped samples, (b) with YSZ and (c) with MSZ.

The use of the ZrO_2 and WO_3 mixtures in a 1:1 and 1:2 ratio for modifying porous mullite ceramics caused the formation of elongated needle-shaped mullite crystals that were randomly located in relation to each other (Figures 5 and 6). Mullite crystals slightly border each other, therefore the structure of the samples is not dense.

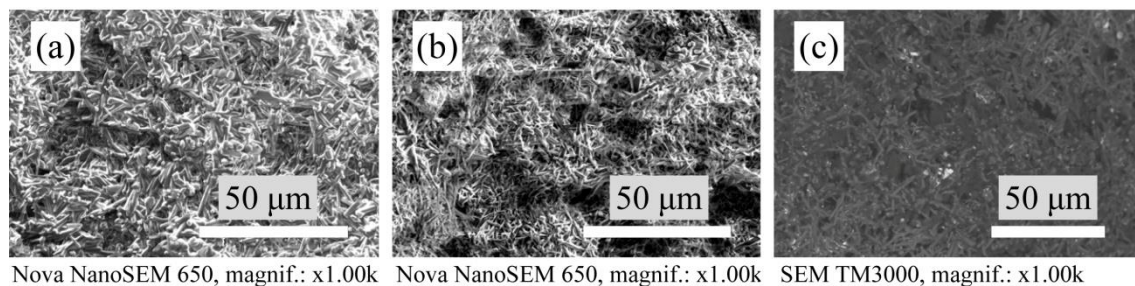


Figure 5. SEM micrographs of the microstructure of sintered samples: (a) with YSZ:WO₃ (1:1), (b) with MSZ:WO₃ (1:1) and (c) with YSZ:WO₃ (1:2).

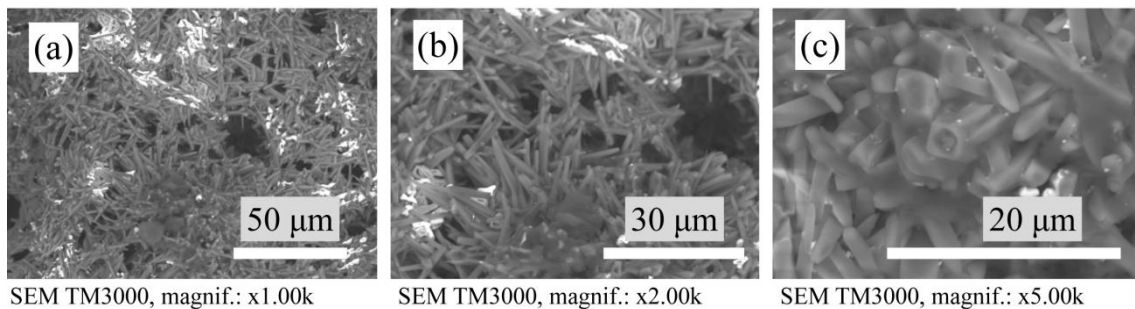


Figure 6. SEM micrographs of the microstructure of sintered samples with MSZ:WO₃ (1:2): (a) magnification $\times 1.00k$, (b) magnification $\times 2.00k$ and (c) magnification $\times 5.00k$.

The samples with a mixture of YSZ:WO₃ and MSZ:WO₃ in a 1:2 ratio have relatively thinner mullite crystals with a distinct acicular or needle-shaped mullite crystals—crystals with a narrow thin ending. The samples with a mixture of MSZ:WO₃ in a 1:2 ratio differ from other sintered materials in that they contain the porous mullite crystals. On the SEM micrographs (Figure 6c), such porous mullite crystals are displayed as elongated needle-shaped crystals with a round hole at the end. It can be assumed that such mullite crystals have internal hollow or voids along the length of the crystals. The formation of hollow mullite crystals occurred due to the formation of the $Al_2(WO_4)_3$ at 1075–1100 °C [48,49] and the presence of the Al–Si–O agglomerations on the surface of the $Al_2(WO_4)_3$ particles. This coincides with the results of the investigations of Liu et al. [49]. The mullitization of such Al–Si–O agglomerations occurred at about 1200 °C, with a simultaneous decomposition of the aluminum tungstate from within. Thus, the porous crystals consisted of a mullite shell and a hollow inner part [49].

3.4. Porosity and Pore Size Distributions

The apparent porosity of the sintered samples is shown in Figure 7. The samples without a modifying additive and samples with a different stabilized zirconia have a similar apparent porosity of about $40 \pm 2\%$. The samples with mixtures of modifying additives have an apparent porosity higher than $59 \pm 2\%$.

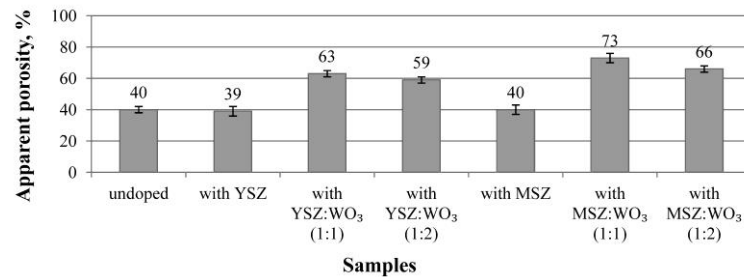


Figure 7. Apparent porosity of the investigated samples.

The use of WO₃ in the equivalent ratio to zirconia noticeably increases the apparent porosity of the samples in comparison with the undoped samples. Porous mullite ceramics modified with magnesia-stabilized zirconia and WO₃ in a 1:1 ratio have the highest apparent porosity ($73 \pm 2\%$). The doubling of WO₃ in the MSZ:WO₃ mixture slightly decreases the porosity ($66 \pm 2\%$) of such samples in comparison with the samples with MSZ and WO₃ in a 1:1 ratio.

The graphs of the pore size distribution after the mercury porosimetry are shown in Figure 8. The undoped samples have three ranges of pore size distributions: 0.05–0.2 μm, 0.3–5 μm and 7–1000 μm, with the most pronounced size of ≈ 0.08 μm, ≈ 0.15 μm and ≈ 150 μm in these ranges (Figure 8a).

Two ranges of pore size distributions are observed for the samples with yttria-stabilized zirconia and magnesia-stabilized zirconia (Figure 8a). The biggest pores of these samples are in range from 20 μm to 500 μm, in which ≈ 150 μm pores are more intensely expressed. Such large pores occupy approximately the same percentage for both compositions. The smaller pores of the samples with the YSZ additive are in the range from 1 μm to 20 μm. For the samples with MSZ, the range of the smaller pores narrows and occupies from approximately 3 μm to 20 μm, and such pores occupy a smaller percentage than in the case of the samples with YSZ. The 5 μm pores are more strongly expressed in the smaller pore size range for the samples of both compositions.

Additionally, the two pore size distribution ranges are in the samples with the YSZ:WO₃ and MSZ:WO₃ mixture in a 1:1 ratio (Figure 8b). The range of the smaller pores expanded with the addition of WO₃, which takes them from 1 to 20 μm, with a pronounced predominance of a 6–7 μm pore size. It can be seen from the graphs in Figure 8b that pores of a smaller diameter (1–20 μm) predominate over the larger sized pores (20–500 μm). The smaller pores of the samples with YSZ:WO₃ (1:1) occupy a slightly bigger percentage as for the samples with MSZ:WO₃ (1:1). The 150 μm pores are more intense in the large size pores range samples with an additional oxide mixture in a 1:1 ratio.

The pore size distributions of the samples with the YSZ:WO₃ and MSZ:WO₃ mixture in a 1:2 ratio are shown in Figure 8c. The doubling of WO₃ decreases the formation of large pores. The range of the large pores takes from 20 μm to 1000 μm. The doubling of WO₃ caused the formation of small pores. The samples with YSZ:WO₃ (1:2) have pores from ≈ 1.5 μm to 20 μm, with primarily 6 μm pores. The pores from 4 μm to 10 μm occupy a significant volume of the samples with MSZ:WO₃ (1:2). The 3–7 μm pores predominate in the case of the samples with MSZ:WO₃ (1:2).

Pores larger than 1000 μm (or 1 mm) are not shown on the pore distribution graphs, although they are shown in the SEM pictures in Figure 3.

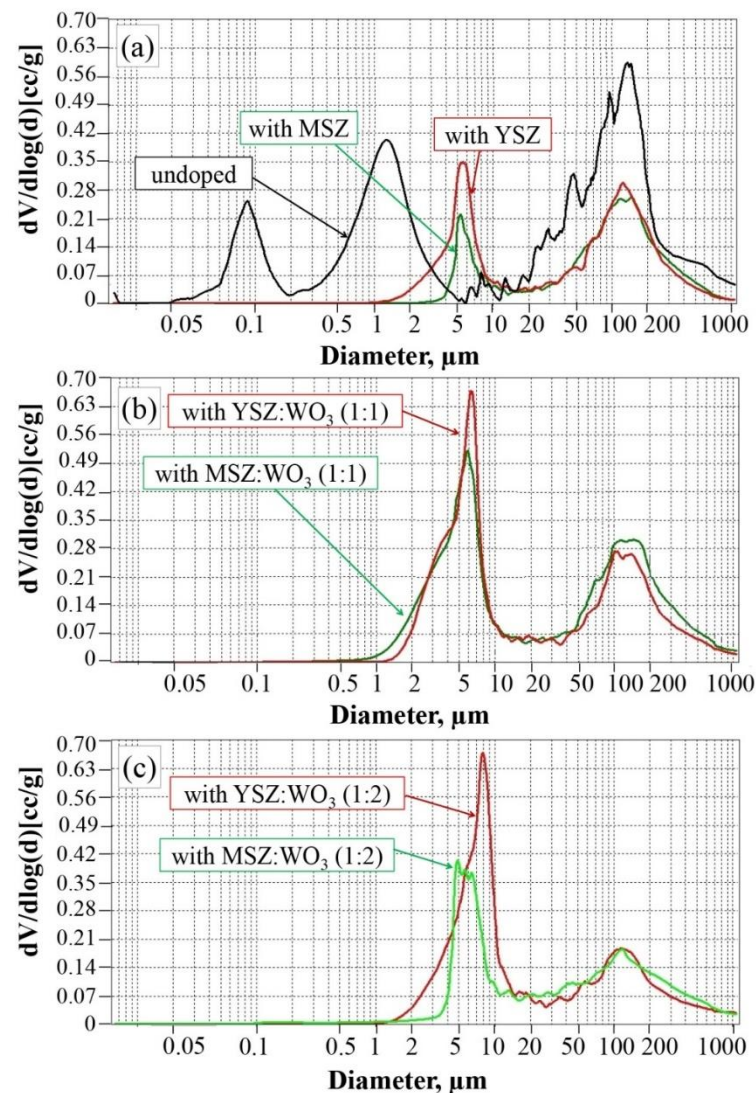


Figure 8. Pore size distributions of the samples: (a) undoped samples, with YSZ and with MSZ; (b) samples with YSZ:WO₃ (1:1) and with MSZ:WO₃ (1:1); and (c) samples with YSZ:WO₃ (1:2) and with MSZ:WO₃ (1:2).

3.5. Specific Heat Capacity

Figure 9 shows the temperature dependence of the specific heat capacity of the investigated samples. The approximately 1200–1300 °C specific heat capacity curves of the mullite single crystals and polycrystalline mullite show an anomalous sigmoidal increase [50], which also corresponds to the specific heat capacity lines obtained for the undoped samples and samples modified with YSZ and MSZ, as well as for YSZ:WO₃ in a 1:1 ratio and MSZ:WO₃ in a 1:2 ratio. These samples have a similar temperature dependence of the specific heat capacity from 25 °C to 1100 °C and an anomalous sigmoidal increase. The specific heat capacity values of the samples with a mixture of YSZ:WO₃ in a 1:2 ratio and a mixture of MSZ:WO₃ in a 1:1 ratio rapidly increase at about 1000 °C and then decrease due to the presence of WO₃ with a characteristic temperature dependence of the specific heat capacity [51–55]. This can be explained by the fact that the phase compositions of these samples have the pronounced presence of the WO₃ phase and its phase transitions during heating. Han et al. determined that the WO₃ phase transitions tetragonal(*t*₁) → tetragonal(*t*₂) at 1200 K (927 °C) occur with a large increase in the specific heat capacity and with a subsequent decrease [52,56–59]. In these works, such an increase in the specific heat capacity of

the porous mullite ceramics occurs closer to 1000 °C perhaps due to the presence of other phases that can affect the phase transition temperature.

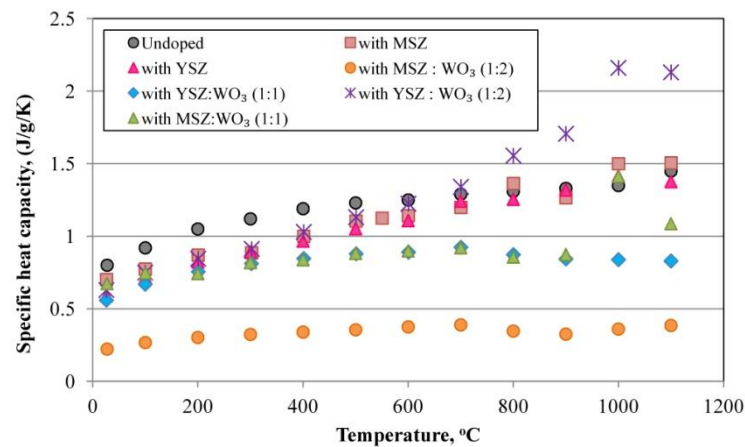


Figure 9. Specific heat capacity of the samples.

The samples with a mixture of MSZ:WO₃ in a 1:2 ratio have the lowest specific heat capacity, which does not exceed ≈ 0.40 J/g/K at all temperature ranges due to the presence of zircon with a relatively low specific heat capacity.

3.6. Thermal Conductivity

Figure 10 shows the thermal conductivity of the sintered porous mullite ceramic samples after the laser flash contactless method measurements. From the point of view of thermal conduction, the porous ceramics can be regarded as a two-phase system [53]. The first phase is the ceramic material skeleton or matrix. The second phase varies as the porosity, pore size and form, as well as the roughness of the pore walls. The heat transfer through such phases forms and describes the common thermal conductivity of the porous ceramic material. The mullite materials are the matrices of the investigated porous ceramics.

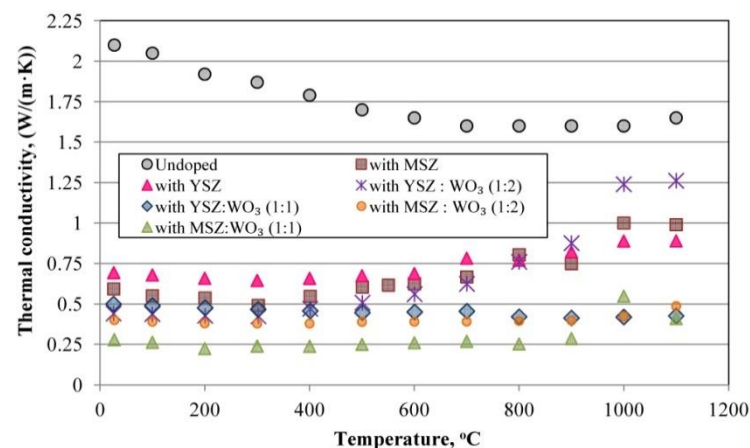


Figure 10. Thermal conductivity of the samples.

The thermal conductivity of the dense fully mullite ceramic is 5.1 W/mK and the thermal conductivity of the air is 0.026 W/mK [53]. The thermal conductivity of the porous mullite ceramics with a porosity of about 75%, according to the published data, is 0.31–0.42 W/mK at room temperature [53]. The thermal conductivity is directly proportional to the porosity of the investigated samples. Samples with a lower porosity of about 39–40% have the highest thermal conductivity, and porous ceramic samples with a porosity of about 63–73% have a lower thermal conductivity.

The undoped samples with a 40% porosity have a higher thermal conductivity in the temperature range of 25–1100 °C compared to all the modified samples. The thermal conductivity of the undoped mullite porous ceramics with a porosity of $\approx 40\%$ is 2.1 W/mK at room temperature. The undoped samples also have a high thermal conductivity due to the predominance of isolated, large-sized spherical pores, as well as due to the presence of a corundum phase with a high $\lambda_{T=25^\circ\text{C}} = 41.9$ W/mK [53,55] that increases the thermal conductivity of the ceramic matrix. The change in the slope on the temperature dependence of the thermal conductivity at temperatures greater than about 1000 °C is due to a radiative contribution to the measured thermal conductivity.

The thermal conductivity of the samples modified with YSZ and MSZ and with a porosity of $\approx 40\%$ at room temperature is 0.69 W/mK and 0.59 W/mK, respectively. The thermal conductivity of such samples with these compositions increased to 0.82 and 0.74 W/mK at 900 °C. Such parameters as the porosity, microstructure and presence of mullite and monoclinic ZrO₂ in the samples only with YSZ or with MSZ are similar, but the thermal conductivity is higher for the samples with YSZ due to the presence of a corundum phase with a high thermal conductivity coefficient. The intensity of the corundum phase of these composition samples is much less than that for the undoped samples, therefore, its influence on the thermal conductivity is less than in the case of the undoped samples.

The thermal conductivity of the samples with a porosity of about 59%, 63% and 66% at room temperature is 0.50 W/mK, 0.40 W/mK and 0.28 W/mK, respectively, for samples with a mixtures of YSZ:WO₃ in a 1:1 and 1:2 ratio and samples with a mixture of MSZ:WO₃ in a 1:2 ratio. Its λ at 900 °C became 0.41 W/mK, 0.40 W/mK and 0.88 W/mK. The thermal conductivity of the samples with a mixture of YSZ:WO₃ in a 1:2 ratio increases with an increasing temperature and became about 0.88 W/mK at 900 °C. The thermal conductivity of the samples with a YSZ:WO₃ mixture in a 1:1 ratio and with MSZ:WO₃ in a 1:2 ratio does not change intensively with an increasing temperature and remains within 0.40 ± 0.02 at 900 °C.

The sintered samples with a MSZ:WO₃ mixture in a 1:1 ratio and with a porosity of 73% have the lowest thermal conductivity of the investigated samples. The thermal conductivity of these samples does not change with an increasing temperature until 900 °C. It is 0.28 W/mK at room temperature and 0.29 W/mK at 900 °C.

Considering the point of view of the so-called mullite ceramic skeleton or matrix, the thermal conductivity is lower for those samples with a looser texture and its structure consists of relatively short, thin, randomly located and loosely packed mullite crystals in the structure. The inclusions of other phase's crystal grains with a low thermal conductivity reduce the overall thermal conductivity of the porous mullite ceramics. This is clearly noticeable in the case of an undoped sample and in the case of a sample with a mixture of MSZ:WO₃ in a 1:1 ratio, respectively, for the samples with the highest and lowest thermal conductivity. The dependence of the grain-size and crystal size on the thermal conductivity cannot be ignored. The thermal conductivity is lower for the samples with smaller and thin crystals, respectively, for the samples with a mixture of MSZ:WO₃ in a 1:1 and 1:2 ratio. This is due to the decrease in the phonon mean free path. As a result, the anharmonic phonon scattering within the grain is dominated and this decreases the thermal conductivity [60].

In its turn, the thermal conductivity is a little higher for the samples with MSZ:WO₃ in a 1:2 ratio than for the samples with MSZ:WO₃ in a 1:1 ratio. The thermal conductivity of the samples with MSZ:WO₃ in a 1:2 ratio is the same at different temperatures, due to the presence of different phases, that prevent the increase in the thermal conductivity with an increasing temperature. The stability of the thermal conductivity of the samples MSZ:WO₃ (1:2) can also be explained by the chaotic arrangement of mullite crystals, which are weakly adjacent to each other. The porous mullite crystals of such samples also decreases the thermal conductivity.

The Increase in the thermal conductivity of the ceramic samples with only YSZ and MSZ or with YSZ:WO₃ in a 1:2 ratio with an increasing temperature from 600 °C to 1000 °C could be explained by the expressed content of the monoclinic ZrO₂. Such an elevation

of the thermal conductivity with an increasing temperature is a characteristic property of zirconium ceramics [61]. For samples with YSZ:WO₃ in a 1:2 ratio, such an increase in the thermal conductivity is also caused by the expressed presence of WO₃. The specific heat capacity and thermal conductivity of WO₃ increases with an increasing temperature [52]. Accordingly, it is less pronounced for the samples with a mixture of YSZ:WO₃ in a 1:1 ratio and MSZ:WO₃ in a 1:1 and 1:2 ratio due to additional phases such as zircon and aluminum tungstate that reduce this effect.

The change in the slope on the temperature dependence of the thermal conductivity at temperatures greater than about 1000 °C is due to a radiative contribution to the measured thermal conductivity.

3.7. Thermal Diffusivity

Figure 11 shows the temperature dependence of the thermal diffusivity of the investigated samples. The undoped samples have the larger thermal diffusivity in comparison with the modified porous mullite ceramics, due to a higher thermal conductivity and the similar specific heat capacity in comparison with the modified samples. These undoped samples potentially faster propagate the heat into the medium.

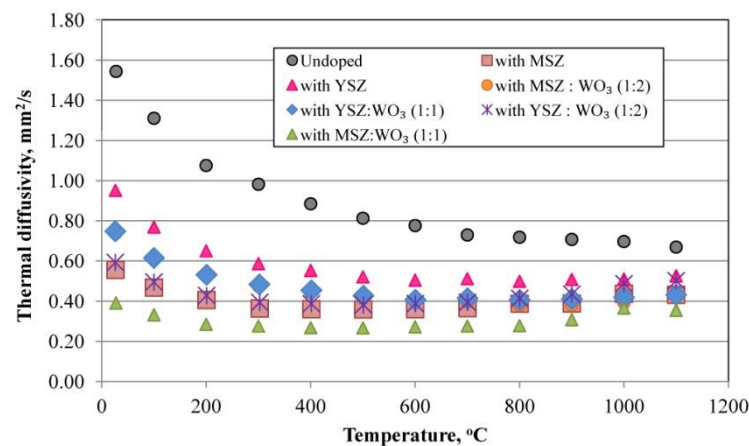


Figure 11. Thermal diffusivity of the samples.

The modified samples have a relatively similar thermal diffusivity. The samples modified with a mixture of MSZ:WO₃ in a 1:1 ratio have a lower thermal diffusivity due to the lower thermal conductivity and relatively low specific heat capacity. The low thermal diffusivity of these samples means that heat is mostly absorbed by the material and a small amount of heat is conducted farther.

3.8. Thermal Shock Resistance

The dependence of the relative change in the elastic modulus on the cycle number of the thermal shock is shown in Figure 12. The undoped samples and samples modified with YSZ and MSZ already have a lower resistance to thermal shock after the first cycle of the temperature change corresponding to the scheme 20 °C → 1000 °C → 20 °C with exposure for 1 h at 1000 °C. Such samples lose more than 15% of the elastic modulus after the 10th cycle due to the induced thermal stress after the rapid temperature change. The reading of the elastic modulus of the samples with YSZ and MSZ improved between the 2nd and 5th cycles due to the process of the crack healing of the ceramic materials. Samples with YSZ and MSZ have the ZrO₂ mainly as a monoclinic (m-ZrO₂) modification but also as tetragonal (t-ZrO₂). With a temperature change from 1000 °C to 20 °C, tetragonal ZrO₂ grains transform into monoclinic grains, thus, the martensitic phase transformation occurs. This phase transformation is accompanied by a volume expansion of 3–4%, which is directed opposite to the crack propagation. The growth of the crack and propagation

were prevented due to the induced compressive stress [21,22,61–64]. However, a further exposure to thermal shock leads to a decrease in the elastic modulus.

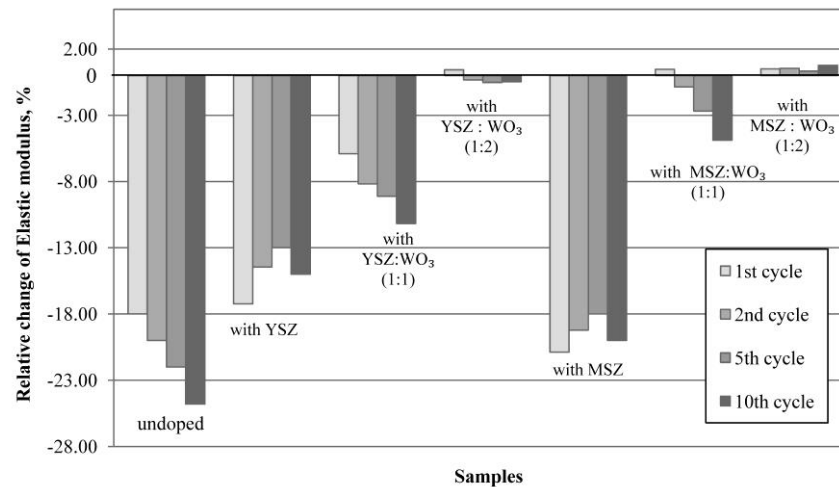


Figure 12. Relative change in the elastic modulus of samples after the thermal shock tests.

The thermal shock resistance of the investigated samples improves with the use of WO_3 in the additive mixture. In the case of the samples with $\text{YSZ}:\text{WO}_3$ in a 1:1 ratio, the relative change in the elastic modulus is negative already after the first thermal shock test and proportionally reduces with the increase in the thermal shock tests' numbers in comparison with the undoped samples and samples with YSZ and MSZ. The relative change in the elastic modulus after the 10th thermal shock cycles is $\approx 11\%$ for the samples with $\text{YSZ}:\text{WO}_3$ in a 1:1 ratio.

The samples doped with a mixture of $\text{MSZ}:\text{WO}_3$ in a 1:1 ratio demonstrate a high resistance to the thermal shock. The elastic modulus of these samples increases by $\approx 0.5\%$ after the 1st thermal shock cycle and decreases within 5% after the 10th cycle.

The samples with a mixture of $\text{YSZ}:\text{WO}_3$ and $\text{MSZ}:\text{WO}_3$ in a 1:2 ratio have a high thermal shock resistance. The elastic modulus of these samples also increases by $\approx 0.4\%$ after the 1st thermal shock cycle, but further behavior is different. In its turn, the elastic modulus of the samples with a mixture of $\text{YSZ}:\text{WO}_3$ in a 1:2 ratio decreases after the 2nd cycle and decreases by 0.5% after the 10th cycle. The elastic modulus of the samples with a mixture of $\text{MSZ}:\text{WO}_3$ in a 1:2 ratio does not decrease. The elastic modulus of such samples increases by 0.5% after the 1st thermal shock test and does not decrease after the 2nd and 5th cycle, but it becomes greater than the initial value by $\approx 0.8\%$ after the 10th cycle.

For samples with a mixture of $\text{MSZ}:\text{WO}_3$ in a 1:1 ratio and a mixture of $\text{YSZ}:\text{WO}_3$ and $\text{MSZ}:\text{WO}_3$ in a 1:2 ratio, the increased thermal shock resistance can be explained by the presence of such crystalline phases as zircon and aluminum tungstate [11,65]. The presence of the aluminum tungstate crystalline phase with a negative linear thermal expansion ($\alpha_{\text{alumin. tungst.}} = -1.5 \times 10^{-6} \text{ }^\circ\text{C}^{-1}$) [48] has an influence on the thermal shock resistance of the investigated ceramics. In the case of the aluminum tungstate phase, it shrinks and allows for the expansion of other the crystalline phases of the investigated ceramic without the formation of the internal stresses in the structure at the thermal shock time. Zircon with its low thermal expansion ($\alpha_{\text{zircon}} = 4.1 \times 10^{-6} \text{ }^\circ\text{C}^{-1}$ from room temperature to $1400 \text{ }^\circ\text{C}$) [65] does not increase the expansion of the ceramic samples.

The samples modified with a mixture of $\text{MSZ}:\text{WO}_3$ in a 1:2 ratio together with the thermal insulating ability show the best thermal shock resistance. The polycrystalline structure with chaotic mullite crystals of these samples and a comparable high porosity of $\approx 63\%$, as well as the presence of small pores with a pore size range from 4 to $10 \text{ } \mu\text{m}$, do not cause the localization of stresses at the moment of the thermal shock. The relatively small branched pores can deflect, slow down or stop the propagation of cracks by its pinning [66].

The elastic modulus does not decrease as a result of a rapid temperature change due to the compensation of stresses and a reduction in the probability of crack formation and growth.

4. Conclusions

The influence of the porous mullite ceramic modification with different micro-sized stabilized ZrO₂ and WO₃ on the thermal properties was investigated. The porous mullite ceramic with a simultaneously low thermal conductivity and high thermal shock resistance was achieved. The following conclusions were reached:

- (a) The use of the micro-sized ZrO₂ and WO₃ additive promotes the formation of elongated partially networked pores with an orientation in a direction parallel to the base of the molds.
- (b) The thermal conductivity decreases with an increasing sample porosity and the randomness of the ceramics structure, as well as with the decreasing mullite crystal thickness.
- (c) The formation of the hollow mullite crystals decreases the thermal conductivity of the ceramics and stabilizes its temperature dependence.
- (d) The increase in the zircon content in the phase compositions of the porous mullite ceramic causes the decrease in the specific heat capacity of these ceramics.
- (e) The presence of zircon and aluminum tungstate in the phase compositions of the porous mullite ceramic improves the thermal shock resistance of the investigated ceramics.

Porous mullite ceramics from raw material compositions with a mixture of magnesia-stabilized zirconia and WO₃ in a 1:2 ratio can be used as a potential thermal-insulating material in conditions of sharp temperature changes.

Author Contributions: Conceptualization, L.M.-G. and V.G.; methodology, L.M.-G., R.S. and V.S.; validation, L.M.-G., M.R. and I.J.; formal analysis, L.M.-G., S.T. and S.F.; investigation, L.M.-G.; resources, L.G. and I.J.; data curation, L.M.-G. and M.R.; writing—original draft preparation, L.M.-G.; writing—review and editing, L.M.-G.; visualization, L.M.-G. and V.G.; supervision, R.S. and V.S.; All authors have read and agreed to the published version of the manuscript.

Funding: This research was funded by the European Regional Development Fund within the Activity 1.1.1.2 “Post-doctoral Research Aid” of the Specific Aid Objective 1.1.1 “To increase the research and innovative capacity of scientific institutions of Latvia and the ability to attract external financing, investing in human resources and infrastructure” of the Operational Programme “Growth and Employment, (No.1.1.1.2/VIAA/1/16/121).

Institutional Review Board Statement: Not applicable.

Informed Consent Statement: Not applicable.

Data Availability Statement: The data presented in this study are available on request from the corresponding author.

Conflicts of Interest: The authors declare no conflict of interest.

References

1. Dedinec, A.; Dedinec, A.; Taseska-Gjorgievska, V.; Markovska, N.; Kanevce, G. Energy transition of a developing country following the pillars of the EU Green Deal. *Therm. Sci.* **2022**, *26*, 1317–1329. [[CrossRef](#)]
2. Salomão, R.; Oliveira, K.; Fernandes, L.; Tiba, P.; Prado, U. Porous refractory ceramics for high-temperature thermal insulation Part 1: The Science Behind Energy Saving. *Interceram Int. Ceram. Rev.* **2021**, *70*, 38–45. [[CrossRef](#)]
3. Medvedovski, E. Alumina–mullite ceramics for structural applications. *Ceram. Int.* **2006**, *32*, 369–375. [[CrossRef](#)]
4. Kurovics, E.; Kulkov, A.S.; Ibrahim, J.-E.F.M.; Kashin, A.D.; Pala, P.; Nagy, V.; Kulkov, S.N.; Gomze, L.A. Mechanical properties of mullite reinforced ceramics composite produced from kaolin and corn starch. *Építőanyag–JSBCM* **2021**, *73*, 149–153. [[CrossRef](#)]
5. Krenzel, T.F.; Schreuer, J.; Laubner, D.; Cichocki, M.; Schneider, H. Thermo-mechanical properties of mullite ceramics: New data. *J. Am. Ceram. Soc.* **2019**, *10*, 416–426. [[CrossRef](#)]
6. Chen, S.; Wang, J.; Yuan, L.; Li, Q. Composite design of low thermal conductivity mullite brick for application to cement kiln. *MATEC Web Conf.* **2018**, *142*, 02008. [[CrossRef](#)]
7. Salomão, R.; Oliveira, K.; Fernandes, L.; Tiba, P.; Prado, U. Porous refractory ceramics for high-temperature thermal insulation—Part 2: The technology behind energy saving. *Interceram Int. Ceram. Rev.* **2022**, *71*, 38–50. [[CrossRef](#)]

8. Wu, D.; Ren, H.; Wang, F.; Wang, H. High temperature thermal insulation performance of light nanomaterials for aerospace craft. *Hangkong Xuebao/Acta Aeronaut. Astronaut. Sin.* **2018**, *39*, 221636.
9. Clarke, D.R. Materials selection guidelines for low thermal conductivity thermal barrier coatings. *Surf. Coat. Technol.* **2003**, *163–164*, 67–74. [[CrossRef](#)]
10. Tavangarian, F.; Hui, D.; Li, G. Crack-healing in ceramics. *Compos. Part B Eng.* **2018**, *144*, 56–87. [[CrossRef](#)]
11. Rendtorff, N.M.; Garrido, L.B.; Aglietti, E.F. Thermal shock resistance and fatigue of Zircon–Mullite composite materials. *Ceram. Int.* **2011**, *137*, 1427–1434. [[CrossRef](#)]
12. Deng, Z.-Y.; Ferreira, J.M.F.; Tanaka, Y.; Isoda, Y. Microstructure and thermal conductivity of porous ZrO₂ ceramics. *Acta Mater.* **2007**, *55*, 3663–3669. [[CrossRef](#)]
13. Lee, W.J.; Cho, Y.J.; Lee, H.S.; Park, I.M.; Park, Y.H. Effect of pore morphology on elastic, heat conduction and thermal shock fracture behaviors of porous ceramics. *Proc. Eng.* **2011**, *10*, 2459–2463. [[CrossRef](#)]
14. Gong, L.; Wang, Y.; Cheng, X.; Zhang, R.; Zhang, H. A novel effective medium theory for modelling the thermal conductivity of porous materials. *Int. J. Heat Mass Transf.* **2014**, *68*, 295–298. [[CrossRef](#)]
15. Belogurova, O.A.; Grishin, N.N. Heat-insulating mullite-cordierite materials made from staurolite. *Refract. Ind. Ceram.* **2013**, *54*, 64–68. [[CrossRef](#)]
16. Angle, J.P.; Wang, Z.; Dames, C.; Mecartney, M.L. Comparison of two-phase thermal conductivity models with experiments on dilute ceramic composites. *J. Am. Ceram. Soc.* **2013**, *96*, 2935–2942. [[CrossRef](#)]
17. Feidt, M. *Finite Physical Dimensions Optimal Thermodynamics 1, From Thermostatistics to Non-Equilibrium Thermodynamics*; Elsevier: Amsterdam, The Netherlands, 2017; ISBN 978-1-78548-232-8.
18. See, A.; Hassan, J.; Hashim, M.; Wahab, Z.A. Thermal diffusivity of kaolinite–mullite ceramic matrix composite with silicon nitride nanoparticle filler. *Thermochim. Acta* **2014**, *593*, 76–81. [[CrossRef](#)]
19. Jannot, Y.; Degiovanni, A. *Thermal Properties Measurement of Materials*; John Wiley & Sons: Hoboken, NJ, USA, 2018; p. 342, ISBN 978-1-119-47505-7.
20. Ilić, S.; Ivanovski, V.N.; Radovanović, Ž.; Egelja, A.; Kokunešoski, M.; Šaponjić, A.; Matović, B. Structural, microstructural and mechanical properties of sintered iron-doped mullite. *Mater. Sci. Eng. B* **2020**, *256*, 114543. [[CrossRef](#)]
21. Aksel, C. The influence of zircon on the mechanical properties and thermal shock behaviour of slip-cast alumina–mullite refractories. *Mater. Lett.* **2002**, *57*, 992–997. [[CrossRef](#)]
22. Kenawy, S.H.; Awaad, M.; Awad, H. In-situ mullite-zirconia composites from kaolin. *Am. Ceram. Soc. Bull.* **2006**, *85*, 9401–9406.
23. Xu, X.; Xu, X.; Wu, J.; Lao, X.; Zhang, Y.; Li, K. Effect of Sm₂O₃ on microstructure, thermal shock resistance and thermal conductivity of cordierite-mullite-corundum composite ceramics for solar heat transmission pipeline. *Ceram. Int.* **2016**, *42*, 13525–13534. [[CrossRef](#)]
24. Li, K.; Ge, S.; Yuan, G.; Zhang, H.; Zhang, J.; He, J.; Jia, Q.; Zhang, S. Effects of V₂O₅ addition on the synthesis of columnar self-reinforced mullite porous ceramics. *Ceram. Int.* **2021**, *47*, 11240–11248. [[CrossRef](#)]
25. Wu, J.; Ding, C.; Xu, X.; Liu, Y.; Wang, Y. Microstructure and performances of corundum–mullite composite ceramics for heat transmission pipelines: Effects of Ho₂O₃ additive content. *Ceram. Int.* **2021**, *47*, 34794–34801. [[CrossRef](#)]
26. Wu, J.; Ding, C.; Xu, X.; Zhou, S.; Zhou, Y.; Zhang, Q. Microstructure and performance of Cd₂O₃ added corundum-mullite ceramics composites for concentrated solar power application. *Ceram. Int.* **2021**, *47*, 17177–17185. [[CrossRef](#)]
27. Gai, K.; Guan, B.; Liang, L.; Li, J.; Wang, Q.; Zhao, T. Continuous aluminum oxide-mullite-hafnium oxide composite ceramic fibers with high strength and thermal stability by melt-spinning from polymer precursor. *J. Eur. Ceram. Soc.* **2022**, *42*, 5911–5921. [[CrossRef](#)]
28. Khorsand, A.; Majidian, H.; Farvizi, M. Wear behavior and microstructure of alumina-mullite- zirconia composites prepared by a novel method: Coating of zircon powder by aluminium alkoxide. *Ceram. Int.* **2022**, *48*, 33594–33603. [[CrossRef](#)]
29. Reinders, L.; Pfeifer, S.; Kröner, S.; Stolpmann, H.; Renftlen, A.; Greiler, L.C.; Clauß, B.; Buchmeiser, M.R. Development of mullite fibers and novel zirconia-toughened mullite fibres for high temperature applications. *J. Eur. Ceram. Soc.* **2021**, *41*, 3570–3580. [[CrossRef](#)]
30. Weinberg, A.V.; Goeuriot, D.; Poirier, J.; Varona, C.; Chaucherie, X. Mullite–zirconia composite for the bonding phase of refractory bricks in hazardous waste incineration rotary kiln. *J. Eur. Ceram. Soc.* **2021**, *41*, 995–1002. [[CrossRef](#)]
31. Kumar, P.; Nath, M.; Ghosh, A.; Tripathi, H.S. Thermo-mechanical properties of mullite–Zirconia composites derived from reaction sintering of zircon and sillimanite beach sand: Effect of CaO. *Trans. Nonferrous Met. Soc. China* **2016**, *26*, 2397–2403. [[CrossRef](#)]
32. Bouchetou, M.L.; Poirier, J.; Morales, L.A.; Chotard, T.; Joubert, O.; Weissenbacher, M. Synthesis of an innovative zirconia-mullite raw material sintered from andalusite and zircon precursors and an evaluation of its corrosion and thermal shock performance. *Ceram. Int.* **2019**, *45*, 12832–12844. [[CrossRef](#)]
33. Rendtorff, N.; Garrido, L.; Aglietti, E. Mullite-zirconia-zircon composites: Properties and thermal shock resistance. *Ceram. Int.* **2009**, *35*, 779–786. [[CrossRef](#)]
34. *ASTM Standards: E 1952–01*; Standard Test Method for Thermal Conductivity and Thermal Diffusivity by Modulated Temperature Differential Scanning Calorimetry. ASTM: West Conshohocken, PA, USA, 2017.
35. Camirand, C.P. Measurement of thermal conductivity by differential scanning calorimetry. *Thermochim. Acta* **2004**, *417*, 1–4. [[CrossRef](#)]

36. ASTM Standards: E1269; Standard Test Method for Determining Specific Heat Capacity by Differential Scanning Calorimetry. ASTM: West Conshohocken, PA, USA, 2018.
37. Robertis, E.D.; Cosme, E.H.H.; Neves, R.S.; Kuznetsov, A.Y.; Campos, A.P.C.; Landi, A.M.; Achete, C.A. Application of the modulated temperature differential scanning calorimetry technique for the determination of the specific heat of copper nanofluids. *Appl. Therm. Eng.* **2012**, *41*, 10–17. [[CrossRef](#)]
38. ASTM Standards: C177-13; Standard Test Method for Steady-State Heat Flux Measurements and Thermal Transmission Properties by Means of the Guarded-Hot-Plate Apparatus. ASTM: West Conshohocken, PA, USA, 2019.
39. ASTM Standards: C1044; Standard Practice for Using a Guarded-Hot-Plate Apparatus or Thin-Heater Apparatus in the Single-Sided Mode. ASTM: West Conshohocken, PA, USA, 2020.
40. ASTM Standards: C1114; Standard Test Method for Steady-State Thermal Transmission Properties by Means of the Thin-Heater Apparatus. ASTM: West Conshohocken, PA, USA, 2019.
41. ASTM Standards: C1113/C1113M-09; Standard Test Method for Thermal Conductivity of Refractories by Hot Wire (Platinum Resistance Thermometer Technique). ASTM: West Conshohocken, PA, USA, 2019.
42. Codorniu, D.M.; Moyano, J.J.; Belmonte, M.; Osendi, M.I.; Miranzo, P. Thermal conduction in three-dimensional printed porous samples by high resolution infrared thermography. *Open Ceram.* **2020**, *4*, 100028. [[CrossRef](#)]
43. ASTM Standards: E1225-13; Standard Test Method for Thermal Conductivity of Solids Using the Guarded-Comparative-Longitudinal Heat Flow Technique. ASTM: West Conshohocken, PA, USA, 2013.
44. ASTM Standarts: E1461; Standard Test Method for Thermal Diffusivity by the Flash Method. ASTM: West Conshohocken, PA, USA, 2022.
45. Rezaee, S.; Ranjbar, K. Thermal conductivity of porous Alumina-20 wt% zirconia ceramic composites. *Ceram. Int.* **2020**, *46*, 16564–16571. [[CrossRef](#)]
46. Zhang, M.; Yang, C.; Zhang, Z.; Tian, W.; Hui, B.; Zhang, J.; Zhang, K. Tungsten oxide polymorphs and their multifunctional applications. *Adv. Coll. Int. Sci.* **2022**, *300*, 102596. [[CrossRef](#)]
47. Mahnicka-Goremikina, L.; Svinka, R.; Svinka, V.; Grase, L.; Goremikins, V. The formation of phases with low or negative linear thermal expansion coefficient in porous mullite ceramics. *Epit&anyag-JSBCM* **2020**, *72*, 91–98. [[CrossRef](#)]
48. Achary, S.N.; Mukherjee, G.D.; Tyagi, A.K.; Vaidya, S.N. Preparation, thermal expansion, high pressure and high temperature behaviour of Al₂(WO₄)₃. *J. Mater. Sci.* **2002**, *37*, 2501–2509. [[CrossRef](#)]
49. Liu, H.; Xiong, X.; Li, M.; Wang, Z.; Wang, X.; Ma, Y.; Yuan, L. Fabrication and properties of mullite thermal insulation materials with in-situ synthesized mullite hollow whiskers. *Ceram. Int.* **2020**, *46*, 14474–14480. [[CrossRef](#)]
50. Girolamo, G.D.; Blasi, C.; Pilloni, L.; Schioppa, M. Microstructural and thermal properties of plasma sprayed mullite coatings. *Ceram. Int.* **2010**, *36*, 1389–1395. [[CrossRef](#)]
51. Chase, M.W., Jr. *NIST-JANAF Thermochemical Tables*, 4th ed.; American Institute of Physics: University Park, ML, USA, 1998; pp. 1–1951.
52. Han, B.-y.; Khoroshilov, A.V.; Tyurin, A.V.; Baranchikov, A.E.; Razumov, M.I.; Ivanova, O.S.; Gavrichev, K.S.; Ivanov, V.K. WO₃ thermodynamic properties at 80–1256 K revisited. *J. Therm. Anal. Calorim.* **2020**, *142*, 1533–1543. [[CrossRef](#)]
53. Gong, L.; Wang, Y.; Cheng, X.; Zhang, R.; Zhang, H. Porous mullite ceramics with low thermal conductivity prepared by foaming and starch consolidation. *J. Porous Mater.* **2014**, *21*, 15–21. [[CrossRef](#)]
54. Manga, M.; Jeanloz, R. Thermal conductivity of corundum and periclase and implications for the lower mantle. *J. Geophys. Res.* **1997**, *102*, 2999–3008. [[CrossRef](#)]
55. Dietrich, B.; Kind, M.; Martin, H. Axial two-phase thermal conductivity of ceramic sponges—Experimental results and correlation. *Int. J. Heat Mass Transf.* **2011**, *54*, 2276–2282. [[CrossRef](#)]
56. Mardare, C.C.; Hassel, A.W. Review on the versatility of tungsten oxide coatings. *Phys. Status Solidi A* **2019**, *216*, 1900047. [[CrossRef](#)]
57. Rao, M.C. Structure and properties of WO₃ thin films for electrochromic device application. *J. Non-Oxide Glasses* **2013**, *5*, 1–8.
58. Zheng, H.; Zhen, O.J.; Strano, M.S.; Kaner, R.B.; Mitchell, A.; Kalantar-zadeh, K. Nanostructured tungsten oxide—Properties, synthesis, and applications. *Adv. Funct. Mater.* **2011**, *21*, 2175–2196. [[CrossRef](#)]
59. Ning, S.; Huberman, S.C.; Ding, Z.; Nahm, Y.-H.; Kim, H.-S.; Chen, G.; Ross, C.A. Anomalous defect dependence of thermal conductivity in epitaxial WO₃. *Adv. Mater.* **2019**, *31*, 1903738. [[CrossRef](#)]
60. Wang, H.; Du, X.; Shi, Y.; Deng, M.; Wang, J.; Qi, J.; Huang, Z. Grain-size dependent thermal conductivity of Gd₂Zr₂O₇ ceramics. *Ceram. Int.* **2022**, *48*, 16444–16448. [[CrossRef](#)]
61. Giordano, R. Machinable zirconia. A study on the building blocks of restorative dentistry. *Inside Dent. Technol.* **2012**, *3*, 1–3.
62. Žmak, I.; Ćorić, D.; Mandić, V.; Ćurković, L. Hardness and indentation fracture toughness of slip cast alumina and alumina-zirconia ceramics. *Materials* **2020**, *13*, 122. [[CrossRef](#)]
63. Banerjee, S.; Mukhopadhyay, P. Chapter 4—Martensitic Transformations. In *Phase Transformations. Examples from Titanium and Zirconium Alloys*; Elsevier: Amsterdam, The Netherlands, 2007; Volume 12, pp. 1–813, ISBN 9780080548791.
64. Zanelli, C.; Dondi, M.; Raimondo, M.; Guarini, G. Phase composition of alumina–mullite–zirconia refractory materials. *J. Eur. Ceram. Soc.* **2010**, *30*, 29–35. [[CrossRef](#)]

-
65. Wei, J.; Bingqiang, H.; Wei, Y.; Li, N.; Miao, Z. Influence of phase evolution and thermal decomposition kinetics on the properties of zircon ceramic. *Ceram. Int.* **2021**, *47*, 27285–27293. [[CrossRef](#)]
 66. Cao, M.C.; Jin, X.X.; Dong, L.M.; Li, X.Y.; Zhang, X.Y. Effect of pore composition on thermal shock resistance of porous ceramics. *Dig. J. Nanomater. Biostructures* **2021**, *16*, 1–9. [[CrossRef](#)]